

# *hp* FINITE ELEMENTS FOR THE SIMULATION OF COUPLED ACOUSTIC-MAGNETO-MECHANICAL SYSTEMS WITH APPLICATION TO MRI SCANNER DESIGN

\*S. Bagwell<sup>1</sup>, P.D. Ledger<sup>1</sup> and A.J. Gil<sup>1</sup>

<sup>1</sup>Zienkiewicz Centre for Computational Engineering, College of Engineering,  
Swansea University, Bay Campus, Swansea SA1 8EN, UK

\*638988@swansea.ac.uk

## ABSTRACT

In this paper, we focus on the generation of a strongly coupled monolithic system to describe the interaction of the magnetic field, generated mechanical vibrations and corresponding acoustic behaviour active in an MRI environment. We linearise the resulting nonlinear equations and consider both temporal and frequency dependant axisymmetric formulations of the full three dimensional problem. We also utilise a stress tensor approach for the electromagnetic forces, previously employed in [1, 2, 3]. This formulation allows the use of  $H^1$  conforming *hp* finite elements, which when combined with *hp* refinement results in the possibility of accurate solutions. The fully discretised scheme is solved by a Newton-Raphson procedure, in an extension of [1], which employed a fixed-point algorithm. The results of our formulation are benchmarked against a series of numerical examples including an application to a realistic magnet geometry shown in Figure 1.

**Key Words:** MRI Scanner; *hp* finite elements; Acoustic Magneto-Mechanical Coupling; Multi physics

## 1. Introduction

Recently Magnetic Resonance Imaging (MRI) has become an important tool in the medical industry. The non-intrusive imaging capability and high resolution makes it desirable for identifying a range of medical ailments, such as tumours, damaged cartilage and internal bleeding. The most common type of magnet used in MRI scanners are superconducting magnets, consisting of superconducting wire cooled by liquid helium contained within a vessel known as a cryostat. Figure 1 shows a typical setup of an MRI scanner, which consists essentially of four main components. A set of main magnetic coils produce a strong uniform stationary magnetic field across the radial section of the scanner. The secondary magnetic coils are used to avoid large stray fields arising outside the scanner. The cryostat consists of a set of metallic vessels used to maintain the supercooled magnet temperatures and shield from radiation. A set of resistive coils inside the imaging volume, known as gradient coils, produce pulsed gradient magnetic fields to generate an image of the patient.

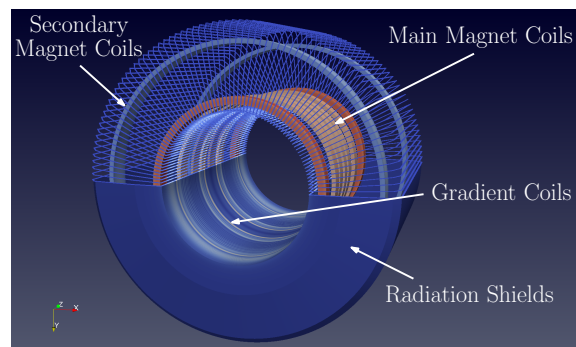


Figure 1: Primary Components of a typical MRI scanner

The presence of eddy currents in these conducting (metallic) vessels can be caused by changing magnetic fields, such as those generated by the pulsed gradient fields. These eddy currents can cause perturbations in the magnetic field. They also give rise to Lorentz forces and exert electro-mechanical stresses in the conducting components which cause them to vibrate and deform. These deformations cause the magnetic field to further perturb thus generating more eddy currents. The vibrations also cause perturbations of the surrounding air, which in turn produces an acoustic pressure field. These phenomena can have undesired effects causing imaging artefacts (ghosting), decreased component life and uncomfortable conditions for the patient, due to the noise from mechanical vibrations.

## 2. Coupled System

The aim of this work is to develop a computational analysis tool to aid in the magnet design by providing a better understanding of the induced vibrations and acoustic behaviour. These phenomena are described through the coupled set of Maxwell (eq. 1a and 1b) and linear elasticity (eq. 1c) equations. In the air the linear elasticity equations reduce to a scalar Helmholtz equation for the acoustic pressure (eq. 1d). Here  $\rho$  denotes the density of the material,  $\mu$  the electromagnetic permeability,  $\epsilon$  dielectric permittivity,  $\gamma$  the electric conductivity,  $\lambda$  and  $G$  the Lamé parameters,  $c$  the speed of sound through a medium,  $\mathbf{E}$  the electric field vector,  $\mathbf{H}$  the magnetic field vector,  $\mathbf{u}$  the displacement field vector,  $\hat{p}$  the acoustic pressure and  $\boldsymbol{\sigma}^m$  is the cauchy stress tensor and the dot symbol ( $\dot{\cdot}$ ) is used to represent a time derivative.

$$\nabla \times \mathbf{E} = \mu \dot{\mathbf{H}} \quad \nabla \cdot \epsilon \mathbf{E} = 0 \quad \text{in } \Omega \quad (1a)$$

$$\nabla \times \mathbf{H} = \mathbf{J}(\dot{\mathbf{u}}, \mathbf{H}, \mathbf{E}) \quad \nabla \cdot \mu \mathbf{H} = 0 \quad \text{in } \Omega \quad (1b)$$

$$\nabla \cdot \boldsymbol{\sigma}^m(\mathbf{u}) + \mathbf{b}(\mathbf{H}) = \rho \ddot{\mathbf{u}} \quad \boldsymbol{\sigma}^m(\mathbf{u}) = \lambda (\nabla \cdot \mathbf{u}) \mathbf{I} + G (\nabla_{sym} \mathbf{u}) \quad \text{in } \Omega_c \quad (1c)$$

$$\nabla^2 \hat{p} - \frac{1}{c^2} \ddot{\hat{p}} = 0 \quad \text{in } \Omega_n \quad (1d)$$

The current term consists of  $\mathbf{J}(\dot{\mathbf{u}}, \mathbf{H}, \mathbf{E}) = \mathbf{J}^s + \mathbf{J}^l(\dot{\mathbf{u}}, \mathbf{H}) + \mathbf{J}^o(\mathbf{E})$ , the source, Lorentz and Ohmic, or eddy currents. The magneto-mechanical coupling, shown in Figure 2, arises in the conductor due to the Lorentz currents and through body forces in terms of Maxwell stresses,  $\mathbf{b}(\mathbf{H}) = \nabla \cdot \boldsymbol{\sigma}^e(\mathbf{H})$  in continuation of [1, 2, 3], defined as

$$\boldsymbol{\sigma}^e(\mathbf{H}) = \mu \left( \mathbf{H} \otimes \mathbf{H} - \frac{1}{2} (\mathbf{H} \cdot \mathbf{H}) \mathbf{I} \right) \quad (2)$$

The acoustic pressure is coupled to the magneto-mechanical problem at the air-conductor interface boundary ( $\partial\Omega_c$ ) through jump conditions in the tractions and accelerations.

$$[[\boldsymbol{\sigma}]] \mathbf{n} = 0 \quad \text{on } \partial\Omega_c \quad (3a)$$

$$[[\ddot{\mathbf{u}}]] = 0 \quad \text{on } \partial\Omega_c \quad (3b)$$

where  $\mathbf{n}$  is the outward normal vector associated with the boundary and the double bracket symbol  $[[x]] = x_n - x_c$  defines the jump in the solution across a boundary. The subscripts c and n correspond to the conducting and non-conducting sub domains of our computational domain, shown in Figure 2.

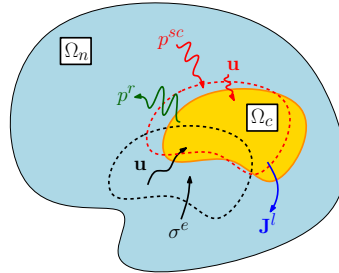


Figure 2: Computational domain of the coupled system

## 3. Computational Framework

### 3.1. Axisymmetric Problem

Given that the geometry of the MRI Cryostat is constant across the bore section of the cylinder and modelling only one set of gradient coils, the Z-gradient, the problem may be expressed in terms of an axisymmetric formulation. By expressing the geometry in cylindrical coordinates the fields are independent of the angular component and so the order of the geometry reduces from 3D to a 2D plane. The problem is solved on the  $r, z$  plane as opposed to the  $x, y, z$  Cartesian domain, whilst still resolving the full 3D nature of the fields. However this requires a more complex weak formulation, which takes account of the differential operators expressed in cylindrical coordinates. By introducing appropriately scaled variables the  $1/r$  singularity at the radial axis can be eliminated and  $u_r$  and  $u_z$  the components of mechanical displacements along with the  $A_\phi$  component of a vector potential for representing the electromagnetic fields can all be discretised by  $H^1$  conforming  $hp$  finite elements.

### 3.2. Time Harmonic System

Computational speed is of great importance to the design process of an MRI scanner, as designers must test a large number of concept designs over a wide range of operational conditions. For this reason one would prefer to solve in the frequency domain, rather than the full time dependant problem. This formulation allows the designer to sweep quickly over the sourcing frequencies of the Z-gradient coil and compute the dissipated power as a function of the frequency. We have therefore chosen to adopt the approach taken in [1] of assuming a time harmonic, rather than pulsed, sourcing current in the gradient coil so that we can formulate the equations in the frequency domain.

### 3.3. Monolithic Scheme

Unlike the work previously carried out in [1], which involves the implementation of a fixed point iteration scheme, we have chosen to adopt a Newton-Raphson approach to solve the coupled system of non-linear equations (eq. 1). By forming the monolithic system, shown below in eq. 4, this method offers a more robust solver with quadratic rates of convergence.

$$\begin{bmatrix} \mathbf{K}_{HH} & \mathbf{K}_{Hu} & \mathbf{0} \\ \mathbf{K}_{uH} & \mathbf{K}_{uu} & \mathbf{K}_{u\hat{p}} \\ \mathbf{0} & \mathbf{K}_{\hat{p}u} & \mathbf{K}_{\hat{p}\hat{p}} \end{bmatrix} \begin{pmatrix} \delta_H \\ \delta_u \\ \delta_{\hat{p}} \end{pmatrix} = - \begin{pmatrix} \mathbf{R}_H(\mathbf{H}, \mathbf{u}) \\ \mathbf{R}_u(\mathbf{H}, \mathbf{u}, \hat{p}) \\ \mathbf{R}_{\hat{p}}(\mathbf{u}, \hat{p}) \end{pmatrix} \quad (4)$$

Where  $\mathbf{R}$  is the system residual vector, obtained from eq. 1,  $\delta$  is the solution update vector and  $\mathbf{K}$  is the Tangent stiffness matrix, formed by taking the directional derivative of the residuals with respect to the solution fields, outlined in [4]. To obtain the solution  $\mathbf{X} = [\mathbf{H}, \mathbf{u}, p]^T$  we define some initial guess  $\mathbf{X}^{[0]}$  and update it by solving eq. 4 and iterating over  $\mathbf{X}^{[k+1]} = \mathbf{X}^{[k]} + \delta$  until convergence is achieved.

### 3.4. Perfectly Matched Layer

Due to the nature of acoustic wave propagation we must treat the infinite boundary of the computational domain with special consideration to allow for accurate results. We have chosen to employ a perfectly matched layer, or PML, to deal with the absorption of outgoing waves and avoid numerical pollution from artificial reflections at the boundary. The PML is analogous to a metamaterial where its parameters are artificial and are constructed through an exponential decay function in the complex plane (resulting in a complex coordinate stretching in the layer), in order to absorb incoming waves. A full PML construction and its behaviour in a  $hp$  finite element context is discussed in [5]. To demonstrate the effect of the PML a simple test problem is setup, shown in Figure 3, in which a sphere is located at the centre of an axisymmetric domain and an incident plane wave is propagated in the positive  $z$  direction (upwards) with a PML around the outer domain boundary. The acoustic pressure can be expressed as  $\hat{p} = \hat{p}^{in} + \hat{p}^{sc}$ , where  $\hat{p}^{in}$  is an incident (known) plane wave and  $\hat{p}^{sc}$  is the unknown scattered wave

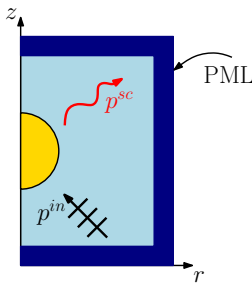


Figure 3: Problem Setup

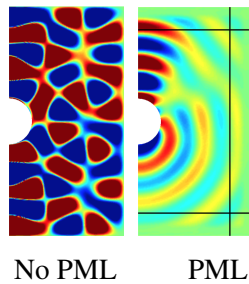


Figure 4: Pressure Field

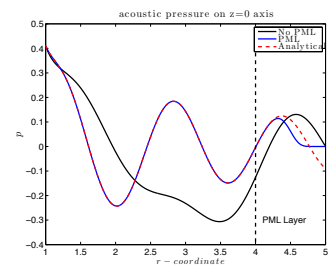


Figure 5: Solution Comparison

The contour plots of the computed scattered field  $\hat{p}^{sc}$  is shown in Figure 4. The left plot shows the pressure field without the PML and the right plot with the PML implemented. Figure 5 is a line plot of the scattered field  $\hat{p}^{sc}$  from the outer radius of the sphere at the centre of the domain to the edge of the PML. It is clear from the plots that without the PML the artificial reflections at the domain boundary cause numerical artefacts to emerge. With the PML implemented it is possible to absorb these waves and allow for accurate solutions within the computational domain. In the PML layer the solution decays to the defined boundary value and does not fully reflect the analytical solution.

#### 4. Numerical Results

We present the following numerical example of a realistic cryostat geometry of an actual MRI scanner. Given that our axisymmetric formulation is still valid for a full 3D problem, Figure 6 shows the plots of the two magnetic field components, generated by the static and gradient coils, around the full 3D scanner.

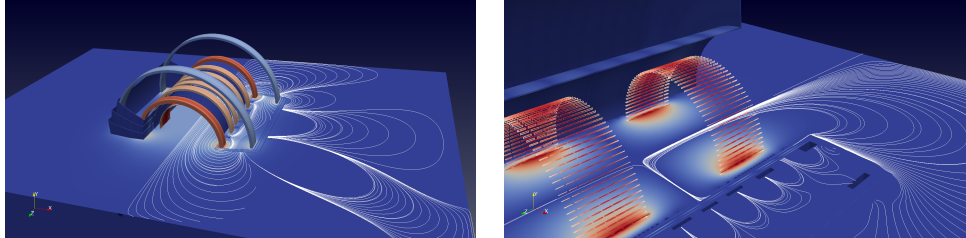


Figure 6: Static (left) and Gradient (right) Magnetic fields

The acoustic behaviour of the MRI magnet geometry is important for determining the noise levels generated during an imaging cycle. The high noise levels can be uncomfortable for patients undergoing a body scan, thus the need to accurately simulate the acoustic pressure generated by the scanner is of vital importance. In Figure 7 the effect of  $p$ , polynomial basis function, refinement on the acoustic distribution is visualised.

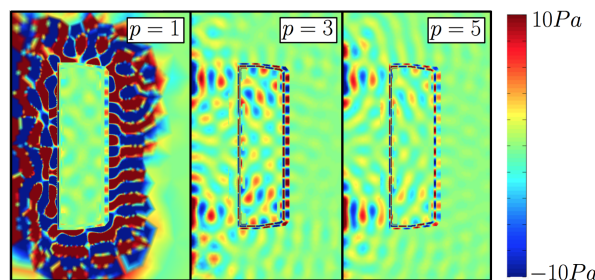


Figure 7:  $p$  effect on acoustic wave problem

The solution for linear,  $p = 1$ , basis functions varies significantly from those with higher order basis functions,  $p = 3$  and  $p = 5$ . The linear shape functions result in numerical dispersion, which causes the amplitude to grow until steady state, whereas the higher order basis functions are much better at capturing the wave function and result in a more accurate solution.

#### 5. Conclusions

The results presented here provide a framework to the set up of an analysis tool for the prediction of deformation and vibration in the conducting regions of an MRI scanner and the corresponding acoustic patterns and sound levels that arise. The accuracy of the non-linear coupled  $hp$  finite element framework has been verified on a series of further benchmark industrial and academic examples, which will be presented in the talk at ACME conference Cardiff.

#### Acknowledgements

The authors gratefully acknowledge the support of EPSRC and Siemens Magnet Technology.

#### References

- [1] P.D. Ledger, A.J. Gil, R. Poya, I. Wilkinson, M. Kruip, S. Bagwell. Solution of an industrially relevant coupled magneto-mechanical problem set on an axisymmetric domain, *Appl Math Model*, Vol. 40, Issue 3, 1959-1971, 2016
- [2] D. Jin, P.D. Ledger, A.J. Gil. An  $hp$ -fem framework for the simulation of electrostrictive and magnetostrictive materials, *Comput Struct vol. 133*, 131-148, 2014
- [3] A.J. Gil and P.D. Ledger, A coupled  $hp$ -finite element scheme for the solution of two-dimensional electrostrictive materials, *Int J Numer Meth Eng*, Vol. 91, Issue 11, 1158-1183, 2012
- [4] J. Bonet and R.D. Wood, Nonlinear Continuum Mechanics for Finite Element Analysis, *Cambridge University Press*, ISBN 978-0-521-83870-2, 1997
- [5] Improving the Performance of Perfectly Matched Layers by Means of  $hp$ -Adaptivity, *Numer Meth Part D E*, Vol. 23, Issue 4, 832-858, 2007